Crystal structure, electric and magnetic properties, and Raman spectroscopy of Gd_3RuO_7

R. P. Bontchev and A. J. Jacobson
Department of Chemistry and Materials Research Science and Engineering Center, University of Houston, Houston, Texas 77204

M. M. Gospodinov
Institute of Solid State Physics, Bulgarian Academy of Sciences, 1184 Sofia, Bulgaria

V. Skumryev
Laboratori de Magnetisme, Departament de Fisica, Universitat Autonoma de Barcelona, 08193 Bellaterra, Spain

V. N. Popov
Faculty of Physics, University of Sofia, 1164 Sofia, Bulgaria

B. Lorenz, R. L. Meng, A. P. Litvinchuk, and M. N. Iliev
Texas Center for Superconductivity and Department of Physics, University of Houston, Houston, Texas 77204-5932
(Received 19 May 2000)

A member of the R_3MO_7 family containing two magnetic cations, Gd_3RuO_7, has been synthesized by high-temperature solid-state reaction. The structure has been determined by single-crystal methods: space group $Cmcm$(#63), $a_0=10.643(2)$ Å, $b_0=7.345(1)$ Å, $c_0=7.380(1)$ Å, $V=576.90(14)$ Å^3, $Z=4$, $R1=0.021$, $wR2=0.047$. The most important structural feature is the one-dimensional RuO_6 chain running parallel to the c axis. In a wide temperature range the conductivity of Gd_3RuO_7 follows the dependence $\ln(\rho)\propto T^{-1/2}$, which is typical for Mott variable-range hopping of localized carriers in one dimension. The magnetic susceptibility obeys the Curie-Weiss law with $\theta_p=-7.5$ K and Curie constant $C_{mol}=25$ emu K/mole. Magnetization data reveal two successive transitions at about 14.5 and 8 K, which indicates independent ordering of Ru and Gd moments, respectively. The analysis shows that in total 27 $(8A_g+8B_{1g}+5B_{2g}+6B_{3g})$ Raman-active modes are expected for Gd_3RuO_7. As a larger number of A_g lines (10) are observed in the polarized Raman spectra, we suggest that two of the A_g lines (at 233 and 780 cm^{-1}) either arise from local vibrations or are of nonphonon origin.

I. INTRODUCTION

Metal oxides of general formula R_3MO_7 (R^{3+}=La, Pr, Nd, Sm, Eu; M^{5+}=Nb, Ta, Sb, Mo, Re, Ru, Ir) have been intensively studied during the last decade.[1–9] This interest is mostly due to the unusual isolated one-dimensional chains formed by corner sharing (MO_6) octahedra, which are present in these structures. Depending on the electronic configuration of the corresponding metals, the resulting materials show some interesting electronic[10,11] and magnetic[12,13] properties. For example, when M^{5+} is a d^0 or d^{10} transition metal, such as Nb, Ta, or Sb, the corresponding oxides are electronically inert.[4,8] When M^{5+} is in a d^n configuration (M=Mo, Re, Ru, Ir; $n=1-4$), the oxide materials are electronically and magnetically active.[1–3,5–7,9] The magnetic properties of these materials could be also modulated as a function of the electronic configuration of the R^{3+} ions. If they contain unpaired electrons, these contribute to the overall magnetic properties and can interact with the magnetic moments of the M^{5+} species.

Ruthenium oxides of the R_3MO_7 type are of particular interest since they contain Ru^{5+} in a d^3 configuration and hence possess the largest possible spin (3/2) among the $4d$ and $5d$ transition metals.[1–3] A typical example is La_3RuO_7 which has been recently synthesized and electronically and magnetically characterized.[1] Since La^{3+} is in the $4f^0$ configuration, the observed magnetic behavior, short- and long-range antiferromagnetic ordering, is only due to Ru^{5+}. Here we report the synthesis, crystal structure, and characterization of a new member of this family, Gd_3RuO_7. It contains two metal species with unpaired electrons [$Gd^{3+}(4f^7)$ and $Ru^{5+}(4d^3)$] and, as expected, shows a complex magnetic behavior.

II. SAMPLES AND EXPERIMENT

A. Synthesis

Polycrystalline Gd_3RuO_7 was prepared by heating a stoichiometric mixture of Gd_2O_3 (Merck, 99.999%) and RuO_2 (Alfa, 99.95%) from 1000 to 1300 °C for 48 h in O_2 with two intermediate regrounds, and finally at 1300 °C in Ar for 24 h. Single crystals were prepared by the polycrystalline Gd_3RuO_7 powder mixed with dried $SrCl_2$ in a mole ratio 1:50 and transferred in a 200 cm^3 platinum crucible. The mixture was heated up to 1300(±0.1)°C (100 deg/h), held for 48 h and than cooled down to 1000 °C with a rate of 1 deg/h. After cooling down to room temperature, the flux was easily removed by repeated washing with hot water, the final product being black prismatic crystals 0.05–0.5 mm in size. Electron microprobe elemental analysis (JEOL JXA-8600, 15 keV) and powder x-ray diffraction (SCINTAG 2000, Cu-K_α radiation) confirmed the stoichiometry and the phase purity of the product.

TABLE I. Atomic coordinates and equivalent isotropic displacement parameters $U(eq)[\text{Å}^2\times10^3]$, defined as one third of the orthogonalized U_{ij} tensor, for Gd_3RuO_7.

Atom	Position	x	y	z	U(eq)
Gd(1)	4*a*	0	0	0	24(1)
Gd(2)	8*g*	0.2241(1)	0.3024(1)	0.25	10(1)
Ru(1)	4*b*	0	0.25	0	5(1)
O(1)	16*h*	0.1282(8)	0.3169(13)	−0.0410(10)	24(1)
O(2)	8*g*	0.1335(8)	0.0271(14)	0.25	13(2)
O(3)	4*c*	0	0.4149(19)	0.25	11(3)
		Selected bond lengths (Å) and angles (deg) for Gd_3RuO_7			
Gd(1)-O(1)		4×2.715(10)	O(1)-Ru-O(1)		89.4(6)
Gd(1)-O(2)		4×2.338(5)	O(1)-Ru-O(3)		85.7(4)
Ru(1)-O(1)		4×1.939(7)	O(3)-Ru-O(3)		180.0
Ru(1)-O(3)		2×1.948(5)	Ru-O(3)-Ru		142.6(4)
Gd(2)-O(1)		2×2.371(7)	O-Gd(1)-O		73.1(3)-108.7(3)
Gd(2)-O(1)		2×2.380(8)	O-Gd(2)-O		65.2(2)-113.4(4)
Gd(2)-O(2)		1×2.241(9)			
Gd(2)-O(2)		1×2.240(9)			
Gd(2)-O(3)		1×2.524(5)			

B. X-ray crystallography

A black polyhedral crystal (0.15×0.06×0.04 mm) was mounted on a SIEMENS SMART single crystal x-ray diffractometer with 1 K CCD area detector. Data were collected using graphite-monochromatized Mo K_α radiation ($\lambda = 0.71073$ Å) at room temperature. A hemisphere of data (1271 frames at 5 cm detector distance) was collected using a narrow-frame method with scan widths of 0.30° in ω and an exposure time of 30 s/frame. The first 50 frames were remeasured at the end of the data collection to monitor instrument and crystal stability and the maximum correction applied on the intensities was <1%. The data were integrated using the Siemens SAINT program[14] with intensities corrections for Lorentz factor, polarization, air absorption, and absorption due to variations in the path length through the detector faceplate. A Ψ scan was used for the absorption correction. The structure was solved by direct methods followed by full matrix least-squares refinement with the SHELXTL software package.[15] A total of 240 independent reflections were collected within the range $3.37° < \theta < 23.23°$. First the Gd and Ru atoms were located and their thermal parameters refined anisotropically. Next the oxygen atoms were located using the difference Fourier map and finally their thermal parameters were refined anisotropically. The main crystallographic data are listed in Table I.

C. Electrical and magnetic measurements

The dc resistivity was measured on pressed powder sample in the temperature range 20–300 K using a standard four-wire technique. Magnetization as a function of temperature and magnetic field was measured on randomly oriented densely packed microcrystals using a superconducting quantum interference device (SQUID) magnetometer (in the range 1.5–300 K) and a vibrating sample magnetometer (in the range 300–500 K). Prior to each run the sample was thermally demagnetized by warming to room temperature. The data reported here were corrected for the demagnetization field effect[19] and for core diamagnetism.

D. Raman spectroscopy

The Raman spectra were measured at room temperature using a spectrometer, equipped with a liquid-nitrogen-cooled CCD (charge-coupled device) and a microscope. The 514.5 nm (Ar^+) or 632.8 nm (He-Ne) laser lines were used for excitation, the laser power in the focus spot (2–3 μm in diameter) being kept below 1 mW to avoid overheating of the sample. An objective of ×100 or ×50 magnification was used both to focus the laser beam on the sample surface and to collect the scattered light.

The samples used for Raman studies were elongated prisms with edges along the [001], [110] and $[1\bar{1}0]$ directions, thus revealing (110) and (001)-type surfaces. Raman spectra therefore could be measured in $y'(zz)\bar{y'}$, $y'(x'z)\bar{y'}$, $y'(x'x')\bar{y'}$, $z(xx)\bar{z}$, $z(xy)\bar{z}$, $z(yy)\bar{z}$, $z(x'x')\bar{z}$, and $z(x'x')\bar{z}$ scattering configurations, where x, y, z, x', and y' denote the [100], [010], [001], [110], and $[1\bar{1}0]$ directions, respectively. Raman studies on polycrystalline samples were also made for comparison.

III. RESULTS AND DISCUSSION

A. Crystal structure

The structure of most of the R_3MO_7 materials has been solved in the orthorhombic space group $Cmcm$(#63),[1–3,5–8] the only exceptions being La_3MoO_7 (space group $P2_12_12_1$)[6] and La_3NbO_7 (space group $Pnma$).[4] For the latter structure, solved by electron-diffraction methods, the authors report a number of weak extra spots which necessarily reduce the cell symmetry from centered (C) to primitive (P).

A careful examination of our data, as well as of an additional set of 20 frames taken at random orientation (exposure time 60 s/frame) showed no extra spots whatsoever, all data being consistent with the reflection conditions for the space group $Cmcm$.[16] Consequently, the structure was solved in this space group, the final cycle of refinement performed on F_0^2 converging at $R1 = 0.021$ and $wR2 = 0.047$. In order to

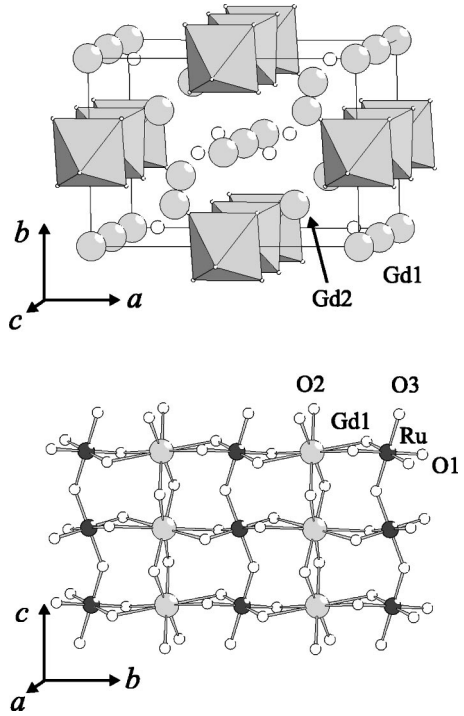

FIG. 1. View of the structure of Gd_3RuO_7 showing the one-dimensional RuO_6 chains (top) and the connectivity within the Gd(1)-Ru-O layers parallel to the *bc* plane. Gadolinium, ruthenium, and oxygen atoms are shown as hatched, filled, and open circles, respectively.

confirm the correctness of this choice, a structure refinement was also carried out in the space group *Pnma*. The most significant difference between the solutions in these two space groups consist of the splitting of one of the oxygen positions in *Cmcm* [O(3), Fig. 1, Table I] in two independent positions in *Pnma*. Our refinement in *Pmna* converged at considerably higher *R* values ($R1=0.065$ and $wR2=0.087$). More important, the thermal parameters of the two oxygen atoms corresponding to O(3) in *Cmcm* were extremely high and the thermal ellipsoids very distorted.

In the structure the ruthenium atoms are coordinated by six oxygen atoms in slightly distorted RuO_6 octahedra (Fig. 1, Table I). The four equatorial Ru-O bonds are of the same length of 1.939(7) Å , the two equivalent apical bonds are slightly longer, 1.948(5) Å , and the O-Ru-O angles vary between 85.7(4) and 94.3(4) deg. The RuO_6 octahedra are joined together in infinite isolated one-dimensional RuO_6 chains by sharing their apical oxygens [O(3)]. The RuO_6 octahedra are tilted with respect to each other with Ru-O(3)-Ru angles of 142.6(4)° and form a zig-zag chain running parallel to the *c* axis (Fig. 1). The ruthenium atoms in two neighboring chains are separated from each other by 7.34 Å along [010] and 10.64 Å along [100] directions, respectively. The closest Ru-Ru distance is 6.47 Å along [220] which indicates that very weak magnetic interactions could be expected between the chains.

The gadolinium atoms are located between the RuO_6 chains and occupy two crystallographically inequivalent positions. The first, Gd(1), is coordinated by eight oxygen atoms forming two sets of four equivalent Gd-O distances of 2.715(10) and 2.338(5) Å , respectively, (Table I, Fig. 1).

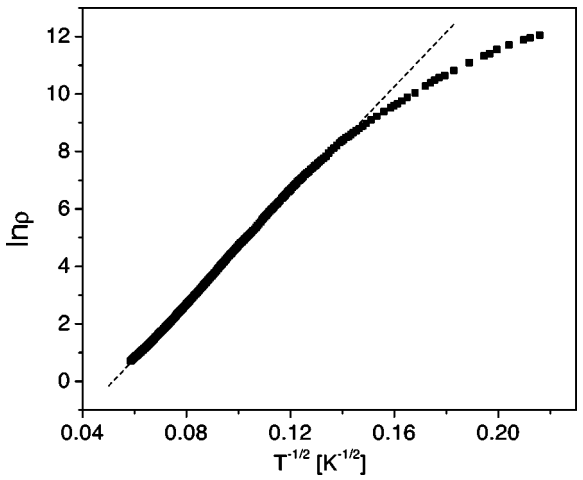

FIG. 2. Temperature dependence of resistivity, $\ln(\rho)$ vs $T^{-1/2}$, between 20 and 300 K for a ceramic sample of Gd_3RuO_7.

The second one, Gd(2), is coordinated by seven oxygen atoms forming Gd-O bonds of five different lengths ranging between 2.240(9) and 2.380(8) Å , (Table I, Fig. 1).

The similarity of the ionic radii of six-coordinated Ru^{5+} and Ir^{5+} (see Ref. 17) allows a comparison of the cell parameters and *M*-O-*M* angles in a series of R_3MO_7 compounds (R^{3+} = La, Pr, Nd, Sm, Gd, Eu; M^{5+} = Ru, Ir).[1–3,5] As expected, the cell volume increases monotonically with the ionic radii of the R^{3+} cations. This increase is reflected in the increase of the *a* parameter, while *b* and *c* remain virtually constant. The values of the *M*-O-*M* angles, which determine the zig-zag pattern of the one dimensional RuO_6 chains, are in the range 140–144 deg. and there is no direct correlation with the ionic radii of the R^{3+} cations.

B. Electrical properties

The room-temperature resistivity was estimated as $2\,\Omega$ cm. With decreasing temperature the resistivity ρ increases up to 200 kΩ cm at 20 K, however, unlike typical semiconductors, the temperature dependence does not follow the Arrhenius law. In a wide temperature range, from room temperature to about 60 K, $\ln(\rho)$ is proportional to $T^{-1/2}$ (Fig. 2). This temperature dependence is typical for Mott variable-range hopping conduction of localized carriers in one dimension.[18] Since the RuO_6 octahedra form a one-dimensional zig-zag pattern, it is reasonable to assume that the main conduction channel is variable-range hopping along the RuO_6 chains. At lower temperatures deviation from the variable-range hopping dependence is observed (Fig. 2).

C. Magnetic properties

The temperature dependence of the magnetic susceptibility, (Fig. 3), obeys the Curie-Weiss law with asymptotic Weiss temperature $\theta_p=-7.5$ K and Curie constant $C_{\mathrm{mol}}=25$ emu K/mole, which is close to the expected value of 25.5, calculated assuming the free ion moment for Gd^{3+} and a high spin $3d^3$ configuration for Ru^{5+}. The high spin configuration of Ru is supported by the recent results of Kalifah *et al.*[1] on the isomorphic La_3RuO_7 compound in which only

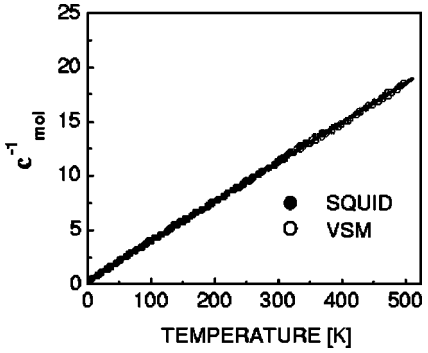

FIG. 3. Temperature dependence of the molar susceptibility of Gd_3RuO_7 at 10 mT. The actual data fit is based on only the more accurate SQUID data.

Ru contributes to the magnetic moment. The negative value of θ_p implies that antiferromagnetic interactions exist between the magnetic moments.

Both zero-field cooled (ZFC) and field cooled (FC) thermomagnetic curves measured in a field of 5 mT (Fig. 4) split below 14.5 K and exhibit a steplike increase of magnetization at about 8 K suggesting two successive transitions. It is plausible to assume that the transition at 14.5 K is due to ordering of the Ru moments, as observed in La_3RuO_7,[1] while the increase of magnetization at about 8 K is related to ordering of the Gd moments.

The initial magnetization curves and the hysteresis loops at different temperatures are given in Fig. 5. The magnetization at 1.5 K shows an initial linear increase up to fields of about 2.2 T [visualized in inset (b)], followed by an upturn of magnetization and stronger field dependence, which tends to saturate at high fields. A small hysteresis is observed at fields below the characteristic value of 2.5 T [see inset (a) in Fig. 5]. The hysteresis loop is characterized with a remanence of 0.12 μ_B/f.u. and coercivity $H_c=0.05$ T. At the same time the $M(H)$ curve at 12 K (a temperature between the two characteristic temperatures marked on the FC-ZFC curves) is convex all the way, with no measurable remanence and coercivity. There is a crossover between the curves at 1.5 and 12 K, the magnetization of the former being smaller than the magnetization of the latter at small fields. This signals an antiferromagnetic coupling at low temperatures with a transition field, as demonstrated on the curve measured at 1.5 K. The magnetic moment at 1.5 K and 12 T is only 18.4 μ_B/f.u., a value much smaller than the expected value of 26.5 μ_B/f.u. for ferromagnetic alignment between Gd and

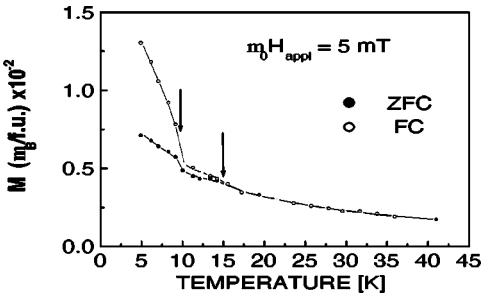

FIG. 4. Zero-field (ZF) and 5 mT field-cooled (FC) thermomagnetic curves measured at $\mu_0 H_{appl}$ of 5 mT.

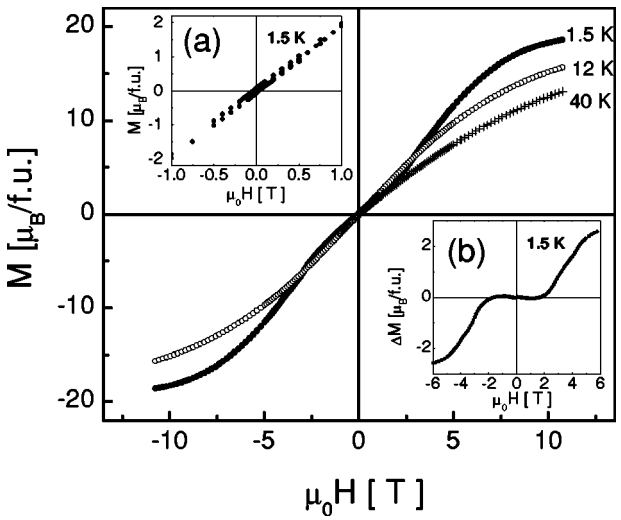

FIG. 5. Magnetization curves of Gd_3RuO_7 at different temperatures (at 40 K, only the first quadrant data are plotted). Note the crossover of the 1.5 and 12 K curves. In inset (b) the linear part of $M(H)$ curve at low fields is subtracted from the $M(H)$ data $[\Delta M(H)=M(H)-M(H)_{linear}]$ to visualize the existence of a critical field of about 2.2 T at which ΔM deviates from zero. An expanded view of the small field region at 1.5 K is presented in the inset (a) to demonstrate the small hysteresis.

Ru moments. A time dependence is observed in the remanence, an effect that deserves further study.

Apart from the above suggested appearance of antiferromagnetism at low temperatures, other explanations of the observed M vs H dependence can also be proposed. Such a behavior could be due to (i) field-induced spin-reorientation when, at a certain field, the moments rotates from one easy direction to another; (ii) domain-wall pinning; (iii) a shape anisotropy associated with the individual elongated crystals. Unfortunately, on the base of our experimental data we cannot determine the true mechanism, although the small remanence seems to contradict to the last two possible mechanisms.

D. Γ-point phonons in Gd_3RuO_7

The results of group-theoretical analysis for the Γ-point phonon modes in Gd_3RuO_7 are summarized in Table II. Out of the total 66 modes, 27 ($8A_g+8B_{1g}+5B_{2g}+6B_{3g}$) are Raman active, 29 ($9B_{1u}+11B_{2u}+9B_{3u}$) are infrared active, 7 ($7A_u$) are silent, and 3 ($B_{1u}+B_{2u}+B_{3u}$) are acoustic modes. As it follows from Table II, the allowed Raman phonon mode symmetries for the scattering configurations available in our experiments are

$$xx,yy,zz \rightarrow A_g,$$

$$x'x'(y'y') \rightarrow A_g+B_{1g},$$

$$x'z(y'z) \rightarrow B_{2g}+B_{3g}$$

$$xy \rightarrow B_{1g}.$$

TABLE II. Wyckoff notations, site symmetries and irreducible representations for the atoms in Gd_3RuO_7 (space group $Cmcm$, No. 63, $Z=4$).

Atom	Wyckoff notation	Site symmetry	Irreducible representations
Gd(1)	4*a*	$C_{2h}^{x}[C_2^{x}+\sigma^{yz}]$	$A_u+2B_{1u}+2B_{2u}+B_{3u}$
Gd(2)	8*g*	$C_s^{xy}[\sigma^{xy}]$	$A_{1g}+A_{2u}+B_{1u}+B_{2g}+2E_g+2E_u$
Ru	4*b*	$C_{2h}^{x}[C_2^{x}+\sigma^{yz}]$	$A_u+2B_{1u}+2B_{2u}+B_{3u}$
O(1)	16*h*	C_1	$3A_g+3A_u+3B_{1g}+3B_{1u}+3B_{2g}+3B_{2u}+3B_{3g}+3B_{3u}$
O(2)	8*g*	$C_s^{xy}[\sigma^{xy}]$	$A_g+A_{2u}+B_{1u}+B_{2g}+2E_g+2E_u$
O(3)	4*c*	$C_{2v}^{y}[C_2^{y}+\sigma^{xy}+\sigma^{yz}]$	$2A_g+B_{1g}B_{1u}+B_{2u}+B_{3g}+B_{3u}$
Selection rules			Modes classification
$A_g\rightarrow\alpha_{xx},\alpha_{yy},\alpha_{zz}$			$\Gamma_{\text{Raman}}=8A_g+8B_{1g}+5B_{2g}+6B_{3g}$
$B_{1g}\rightarrow\alpha_{xy}$			$\Gamma_{\text{ir}}=10B_{1u}+12B_{2u}+10B_{3u}$
$B_{2g}\rightarrow\alpha_{xz}$			$\Gamma_{\text{silent}}=7A_u$
$B_{3g}\rightarrow\alpha_{yz}$			$\Gamma_{\text{acoustic}}=B_{1u}+B_{2u}+B_{3u}$

E. Raman spectroscopy

Figure 6 shows the Raman spectra of Gd_3RuO_7 measured at room temperature in several exact scattering configurations using 632.8 nm (upper panel) and 514.4 nm (lower panel) excitations. The polarization of the Raman lines allows unambiguous assignment to modes of either A_g or B_{1g} symmetry. No spectral structures could be detected in the $x'z$ spectra, which shows that the Raman lines corresponding to the modes of B_{2g} or B_{3g} symmetry are of much lower intensity. It follows from Fig. 6 that in total ten Raman lines of A_g symmetry are observed at 134, 233, 270, 373, 389, 414, 488, 560, 690, and 780 cm^{-1}. As only eight A_g modes are expected for the $Cmcm$ structure, at least two of these lines are either due to local modes, or are of nonphonon origin. Compared to the other Raman lines, the A_g lines at 233 and 780 cm^{-1} exhibit anomalous temperature behavior: the former hardens with increasing temperature between 300 and 400 K, whereas the latter disappears in the same temperature range. Both lines are observed with 632.8 nm, but not with 514.5 nm excitation. The possibility to relate these sharp lines to crystal-field excitation or luminescence of Gd^{3+} has to be ruled out as the Gd^{3+} ion has a singlet ground state and the first excited multiplet is high above the laser excitation energy.

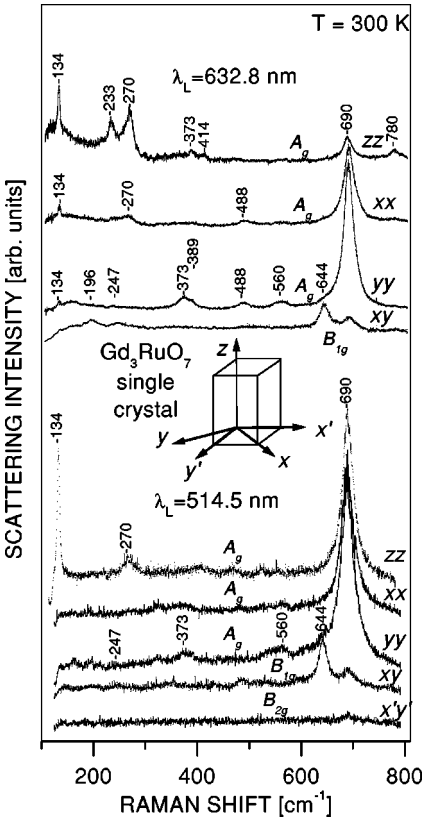

FIG. 6. Polarized Raman spectra of Gd_3RuO_7 at room temperature measured in several exact scattering configurations with 632.8 nm (upper panel) and 514.5 nm (lower panel) excitation.

An assignment of the Raman lines to definite atomic vibrations can be made by comparison with the results of lattice-dynamical calculations and experimental Raman spectra of some isostructural R_3RuO_3 and Gd_3MO_3 compounds. Such calculations and measurements are now in progress. The preliminary results show that only few lines correspond to modes of relatively simple shape. The A_g line at 134 cm^{-1} arises from a mode involving mainly vibrations of Gd(2) along *x*. The most intense A_g(690 cm^{-1}) and B_{1g} (644 cm^{-1}) lines are related to the stretching and antistretching vibrations of $Ru[O(1)]_4$ squares, respectively.

IV. CONCLUSIONS

The compound Gd_3RuO_7, has been synthesized in the form of separate single microcrystals and ceramics. Its structure, as determined by single-crystal methods, is described by the orthorhombic $Cmcm$ space group and contains one-dimensional RuO_6 chains running parallel to the *c* axis. The conductivity of Gd_3RuO_7 follows the dependence $\ln(\rho)\propto T^{-1/2}$, which is typical for Mott variable-range hopping of localized carriers in one dimension. Magnetic susceptibility of Gd_3RuO_7, which obeys the Curie-Weis law, implies that antiferromagnetic interactions exist between the magnetic moments and that Ru^{5+}, as expected for this compound, is in a high spin configuration. Two successive transitions, at 14.5

and 8 K, take place with decreasing temperature. This suggests an independent ordering of Ru and Gd moments and an antiferromagnetic coupling at very low temperatures with a transition field. The present magnetic results call for more detailed studies, involving complementary experimental techniques, to determine precisely the magnetic structure at different temperatures as well as the interactions, if any, between Gd and Ru sublattices. The polarized Raman spectra are consistent with the $Cmcm$ structure, although two extra lines with A_g symmetry are observed with 632.8 nm excitation. These lines (at 233 and 780 cm^{-1}) exhibit anomalous temperature behavior and their assignment requires further investigation.

ACKNOWLEDGMENTS

We thank the Texas Center for Superconductivity and the Robert A. Welch Foundation for support of this work. This work was also supported by the MRSEC program of the National Science Foundation under Award No. DMR-9632667. The work of M.M.G. was supported by the Bulgarian National Science Foundation under Award No. F-701. V.S. wishes to thank the Generalitat de Catalunya for a grant. We are grateful to J. Cmaidalka and S. G. Dobreva for help in sample preparation. We also thank Y. Y. Xue, Y. Y. Sun, M. Abrashev, V. Hadjiev, L. Ranno, B. Martinez, and J. Nogués for the help with some of the measurements and for numerous helpful discussions.

[1] P. Khalifah, R.W. Erwin, J.W. Lynn, Q. Huang, B. Batlog, and R.J. Cava, Phys. Rev. B **60**, 9573 (1999).
[2] F.P.F. van Berkel and D.J.W. Ijdo, Mater. Res. Bull. **21**, 1103 (1986).
[3] W.A. Groen, F.P.F. van Berkel, and D.J.W. Ijdo, Acta Crystallogr., Sect. C: Cryst. Struct. Commun. **43**, 2262 (1987).
[4] A. Kahn-Harari, L. Mazerolles, D. Michel, and F. Robert, J. Solid State Chem. **116**, 103 (1995).
[5] J.F. Vente and D.J.W. Ijdo, Mater. Res. Bull. **26**, 1255 (1991).
[6] J.E. Greedan, N.P. Raju, A. Wegner, P. Gougeon, and J. Padiou, J. Solid State Chem. **129**, 320 (1997).
[7] G. Wltchek, H. Paulus, I. Svoboda, H. Ehrenberg, and H. Fuess, J. Solid State Chem. **125**, 1 (1996).
[8] J.F. Vente, R.B. Helmholdt, and D.J.W. Ijdo, J. Solid State Chem. **108**, 18 (1994).
[9] F. Wiss, N.P. Raju, A.S. Wills, and J.E. Greedan, Int. J. Inorg. Mater. **2**, 53 (2000).
[10] P. Monceau, N.P. Ong, A.M. Portis, A. Meerschaut, and J. Rouxell, Phys. Rev. Lett. **37**, 602 (1976).
[11] J. Dumas, C. Schlenker, J. Marcus, and R. Buder, Phys. Rev. Lett. **50**, 757 (1983).
[12] J.P. Boucher and L.P. Regnault, J. Phys. I **6**, 1939 (1996).
[13] M. Isobe and Y. Ueda, J. Phys. Soc. Jpn. **65**, 1178 (1996).
[14] SAINT, Version 4.05, Siemens Analytical X-ray Instruments, Madison, WI, 1995.
[15] G. M. Sheldrick, SHELXTL, Version 5.03, Siemens Analytical X-ray Instruments, Madison, WI , 1995.
[16] *International Tables for Crystallography*, Vol. A, 3rd revised ed., edited by T. Hahn (Kluwer Academic, London, 1992).
[17] R.D. Shannon, Acta Crystallogr., Sect. A: Cryst. Phys., Diffr., Theor. Gen. Crystallogr. **32**, 751 (1976).
[18] N. F. Mott and E. A. Davis, *Electronic Proceses in Noncrystalline Materials*, 2nd ed. (Clarendon, Oxford, 1979).
[19] D.-X. Chen, J.A. Brug, and R.B. Goldfarb, IEEE Trans. Magn. **27**, 3601 (1991).